AGU ADVANCING EARTH AND SPACE SCIENCES

Earth and Space Science

RESEARCH ARTICLE
10.1029/2023EA003326

Key Points:

- Non-seasonal vertical ground displacements are used to measure interannual terrestrial water storage variations
- Interannual changes of vertical displacements are a reliable near real-time indicator of drought severity
- The inversion of Global Navigation Satellite System displacements shows that about 70 billion tons of water is lost during the 2021–2022 drought in the Po river basin

Supporting Information:

Supporting Information may be found in the online version of this article.

Correspondence to:

F. Pintori,
francesco.pintori@ingv.it

Citation:

Pintori, F., & Serpelloni, E. (2024). Drought-induced vertical displacements and water loss in the Po river basin (Northern Italy) from GNSS measurements. *Earth and Space Science*, *11*, e2023EA003326. https://doi.org/10.1029/2023EA003326

Received 25 OCT 2023
Accepted 8 DEC 2023

Author Contributions:

Conceptualization: F. Pintori, E. Serpelloni
Formal analysis: F. Pintori
Investigation: F. Pintori
Methodology: F. Pintori, E. Serpelloni
Supervision: E. Serpelloni
Validation: F. Pintori
Writing – original draft: F. Pintori, E. Serpelloni

Drought-Induced Vertical Displacements and Water Loss in the Po River Basin (Northern Italy) From GNSS Measurements

F. Pintori[1] **and E. Serpelloni**[1]

[1]Istituto Nazionale di Geofisica e Vulcanologia (INGV), Bologna, Italy

Abstract We study vertical ground displacement time series from Global Navigation Satellite System (GNSS) stations to measure deformation associated with hydrological drought in the Po river basin. Focusing on interannual trend changes, rather than seasonal (annual) components, we found a clear spatially correlated deformation signal that is temporally (anti)correlated with changes in the Po river level and the SPEI-12 drought index, with stations moving upward during periods of river/index level decrease and vice versa. In the 2021–2022 time span, which culminated in the most severe drought of the last two centuries, we estimate the amount and spatial distribution of water loss in the basin and its surroundings. Excluding the seasonal signals, between January 2021 and August 2022, the GNSS stations underwent uplift, up to 7 mm, which corresponds to ∼70 Gtons of water loss. Compared to Global Land Data Assimilation System and Gravity Recovery and Climate Experiment estimates, GNSS results show a similar temporal evolution of water content but a more heterogeneous distribution of values. We show that continuous GNSS networks provide an effective way to monitor multiannual trend changes in water storage even in small water basins and serve as a reliable indicator of drought severity.

Plain Language Summary This study looks at the way the ground moves up and down in the Po river basin, in northern Italy, using Global Navigation Satellite System (GNSS) stations. We measure how much water was lost during a big drought in the area, which occurred from January 2021 to August 2022. During this time interval, the GNSS stations show that the ground mostly moved upwards, which means that water was being lost. Besides the annual water storage variations, we estimate that about 70 billion tons was lost during that time, in agreement with other ways of measuring terrestrial water variations. This study shows that GNSS stations can be an alternative way to measure how much water is being lost during drought in small areas and common vertical displacement signals are a good approximation of drought indexes.

1. Introduction

Drought is one of the most complex recurring natural disasters, defined by a deficiency of precipitations that causes prolonged water scarcity. Failure to manage drought risk has the potential to have dire consequences for people, livelihoods, economy and ecosystems. During the summer of 2022, Italy faced the most severe drought in the last two centuries, where the dry conditions were related to several drivers, the most relevant being the changes in the precipitation regime, resulting in a decline of snow fraction and snowmelt, and an increasing evaporation rate (Montanari et al., 2023). The drought significantly impacted the largest Italian river, the Po, whose level has significantly decreased from the summer of 2021 to the autumn of 2022 (Figure 1). In summer 2022 several regions declared a state of emergency, and drinking water has been rationed in hundreds municipalities in northern Italy.

The effects of droughts are particularly dangerous in the Po river basin, which has an extension of $\sim 74 \cdot 10^4$ km^2, for various reasons: drought threatens the crops in the Po Valley, which are around 40% of the total food produced in Italy, and impacts energy production, since a reduced river flow causes deficiencies in hydropower generation and cooling of thermal plants (Boyko et al., 2022).

Due to global warming, more frequent, longer and severe droughts are likely to occur in the future (Boyko et al., 2022). In order to evaluate the best policies to address the problems caused by water scarcity, it is crucial to measure and monitor variations in terrestrial water storage (TWS). For drought monitoring, in fact, changes or anomalies in TWS provide direct observations of total water availability, complementing model-based measures

Writing – review & editing: F. Pintori, E. Serpelloni

such as drought severity indices. Taking into account the anomalies of both precipitation and potential evapotranspiration, Vicente-Serrano et al. (2010) proposed the Standardized Precipitation-Evapotranspiration Index (SPEI) drought index. However, meteorological drought indices, such as the SPEI, and other drought indices, like the Standardized Precipitation Index or the Palmer Drought Severity Index, estimate droughts based on precipitation and temperature anomalies, so they do not allow to quantify TWS anomalies. TWS, in general, is hard to quantify because it is the sum of many components, including groundwater, surface water, vegetation and soil moisture, ice and snow. Piezometers, for example, effectively monitor groundwater level variations but not the other water storage components, and evaluating the water volume changes from them is not straightforward. On the other hand, the Global Land Data Assimilation System (GLDAS) model provides daily variations of the soil moisture and snow water equivalent, but it can not take into account the groundwater stored more than 2 m below the surface (Argus et al., 2014; Jiang et al., 2021). Geodetic techniques have a distinctive role in monitoring the hydrological cycle, as they are the sole means of directly observing TWS anomalies and they can function across local to global scales. TWS anomalies can be estimated at global scale by using Gravity Recovery and Climate Experiment (GRACE) measurements, which allow modeling water storage changes by inverting the spatiotemporal variations of the Earth's gravity field. Unlike GLDAS, GRACE accounts for all the components of TWS, but it provides a spatial resolution of ∼300 km, which is insufficient for monitoring smaller watersheds (Fu et al., 2015; Knappe et al., 2019), particularly in mountainous regions where TWS gradients are steep, as highlighted in Argus et al. (2017). Moreover, due to the monthly nature of GRACE observations they are not suitable for assessing water availability and flood risk during and following brief, intense precipitation events.

TWS variations are indirectly detectable not only through gravity data but also by measuring ground deformation through geodetic observations: an increase of the water content, in the absence of poroelastic processes, causes an increasing load on the Earth surface, which subsides elastically; while when the water content decreases the crust moves upward because of the water content decrease. Global Navigation Satellite System (GNSS) measurements, for example, provide daily measurements of ground displacements, at mm precisions, that can be used to measure ground deformation associated with TWS variations and then to quantify the severity of a hydrological drought. Argus et al. (2014) inferred the spatial distribution of the TWS seasonal amplitude, expressed in terms of equivalent water height (EWH), by inverting the seasonal vertical displacements of the ground in California, while Ferreira et al. (2019) performed a similar analysis considering the entire South America. Fu et al. (2015) estimated TWS variations from GNSS measurements of vertical displacement in Washington and Oregon, finding that the largest seasonal variations of water content were localized in the mountain areas.

GNSS displacements have been inverted also to characterize hydrological droughts: Jiang, Hsu, Yuan, Tang, et al. (2022) produced a drought severity index, in the contiguous United States, based on GNSS-measured hydrological loading displacements, which was used also by Zhu et al. (2023) over the Yunnan Province in China.

Carlson et al. (2022) computed TWS variations in California using a joint inversion method combining the GRACE products with the results of the inversion of GNSS data, taking advantage of the dense spatial distribution of GNSS data together with GRACE's ability to provide regional closure of the water budget. While most of the above mentioned studies dealt with seasonal fluctuations of TWS, here we focus on multi-annual trends. We model displacement time-series looking for trend changes in the vertical component, with the goal of studying vertical trend changes caused by interannual TWS variations, similarly to Borsa et al. (2014), focusing in particular on the most recent and severe 2021–2022 drought.

In Section 2 we describe the GNSS data used and the methods applied to analyze the vertical displacement time series; in Section 3 we show the relationship between geodetic and hydrological observations and provide a quantitative estimation of the evolution of the TWS. In Section 4 we discuss the results, in light of alternative estimates of water storage variations.

2. Data and Methods

We consider ∼180 daily GNSS vertical ground displacement time series from January 2010 to June 2023 of continuous stations located in the Po river basin (see Figure 1). We also include in the analysis ∼280 stations located within 1° of the catchment limits in order to reduce inversion artifacts near the boundaries of the study region (Fu et al., 2015). This is part of a larger geodetic solution encompassing the whole Euro-Mediterranean region, obtained following the approach detailed in Serpelloni et al. (2022). We remove the long-term linear trend from the time series using the Median Interannual Difference Adjusted for Skewness (MIDAS) estimator (Blewitt et al., 2016) and filter the contribution of the non-tidal atmospheric loading (NTAL), as suggested by

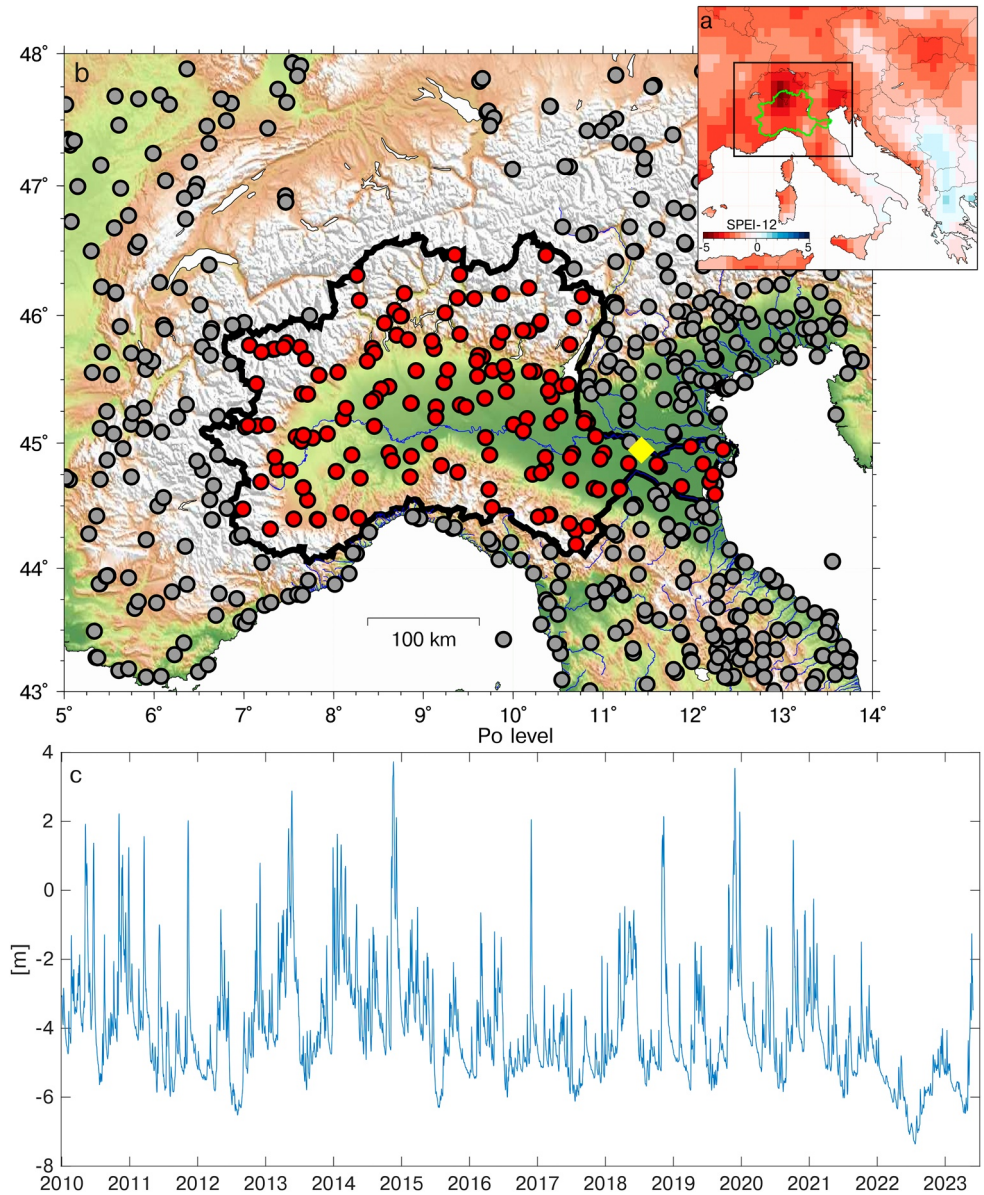

Figure 1. (a) Map of the SPEI-12 values at August 2022. (b) The study area: the black line represents the Po river (thick blue line) basin; the dots show the positions of the Global Navigation Satellite System stations used in the analysis, the reds are the ones inside the basin, the gray the ones outside; the yellow diamond shows the location of the Po level measurement point. (c) Po river level changes.

White et al. (2022), since they can produce displacements of several millimeters at daily weekly timescales that can interfere with the hydrological signal. The NTAL-induced vertical displacements are evaluated from the daily 0.5° × 0.5° gridded solution of the Earth-System-Modeling Group at the German Research Center for Geosciences (Dill & Dobslaw, 2013) and its contribution in each site is calculated considering the nearest grid point where the displacements associated with NTAL are computed.

The resulting GNSS vertical displacements time series are then analyzed using a trend filtering approach, which performs an extensive analysis using a L1 norm regularization model to identify the seasonal components, offsets and linear trend changepoints in the GNSS time series (Wu et al., 2018). The piecewise trend is estimated by minimizing the weighted sum objective function:

$$(1/2)\|y - x - s - w\|_2^2 + \lambda\|D^{(2)}x\|_1 + \rho\|D^{(1)}w\|_1$$

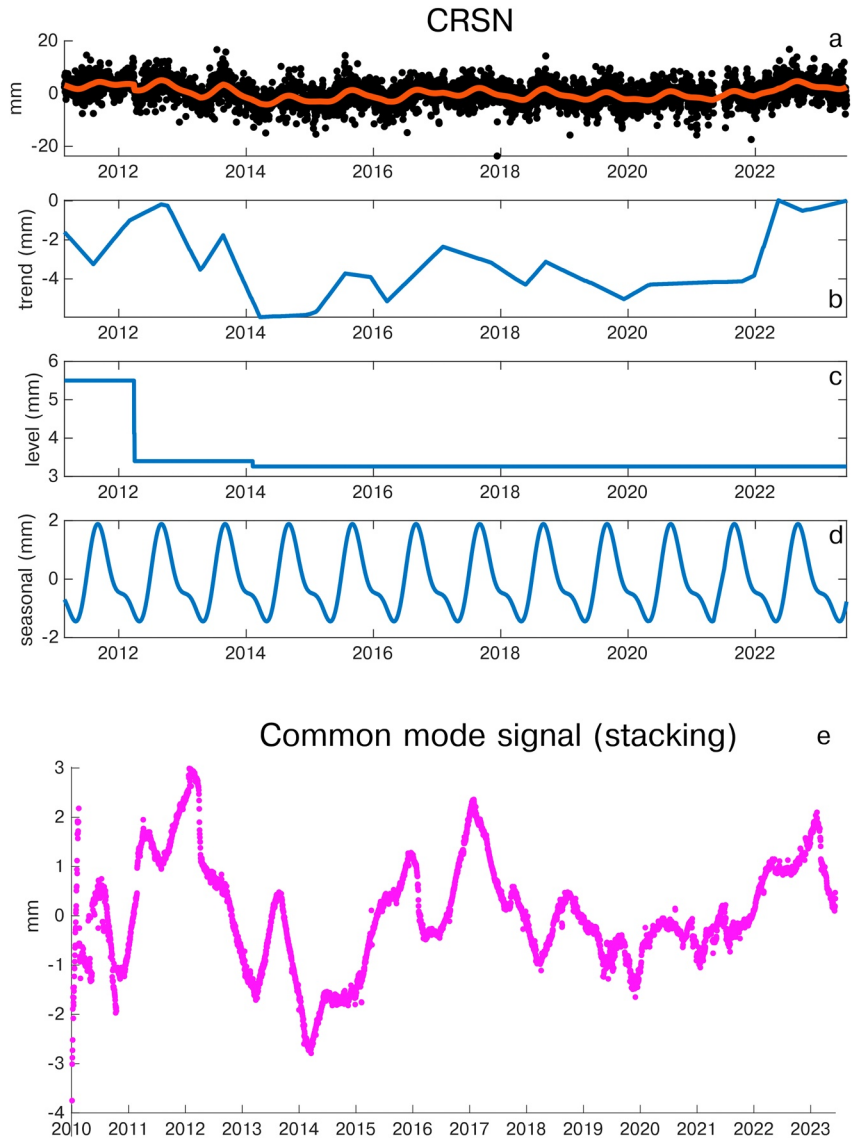

Figure 2. Example of Global Navigation Satellite System time series decomposition performed using the L1-norm trend filtering approach. In (a) the black dots represent the original time series, the red line the model obtained as the sum of the trend (b), level (c) and seasonal component (d). Panel (e) shows the result of the stacking on the piecewise vertical trends of all the stations inside the Po river basin.

where y is the original time series, w indicates the level component associated with the offsets, s is the seasonal term, $\|.\|_1$ represents the L1 norm and $D^{(n)}$ are the n-th difference matrix defined as in Wu et al. (2018). λ and ρ are positive parameters controlling the knots of the estimation trend and the frequency of level shifts, respectively (we choose $\lambda = 2000$ and $\rho = 80$). Figure 2 shows an example of output of this analysis. Focusing on transients and interannual variations, we only consider the extracted piecewise trends, not the seasonal terms having annual and semi-annual frequencies. For some stations level changes (i.e., offsets) not associated with tectonic events or equipment changes are highlighted, which mostly represent fast variations in ground displacements (see Figure 2 in 2012). For this reason, in the further steps we consider the piecewise trend as the sum of the trend and level components. As it can be seen in Figure 2, there is an increase in uplift starting from 2021, which is a common feature in GNSS stations within the Po river basin. Figure 2e shows the stacking of the vertical piecewise trend time-series for all stations analyzed, which is performed by averaging, for each epoch, the residuals of all the time series resulting by removing the mean and linear trend terms. In order to better characterize the spatial distribution of this deformation signal, we use a multivariate statistical approach, similarly to what is used for tectonic deformation studies (Gualandi et al., 2014; Kositsky and Avouac, 2010).

3. Results

3.1. Comparison Between Geodetic and Hydrological Measurements

We adopt an approach similar to the one described in Jiang, Hsu, Yuan, Feng, et al. (2022), but using as input of a principal component analysis (PCA) the piecewise vertical trends described in the previous section rather than the raw time-series that also include the seasonal terms. We decompose the data set using one PC in order to identify the most important common signal of the GNSS stations in the Po basin and retrieve its spatial pattern (i.e., amplitude and sign). However, the first principal component (PC1) obtained performing a PCA using two components is almost identical to the PC1 obtained performing a one-component decomposition, both in terms of temporal evolution (Figure S1 in Supporting Information S1) and spatial distributions (Figure S2 in Supporting Information S1).

The temporal evolution of PC1 (Figure 3a) well resembles the common mode signal resulting from a stacking of the vertical trend time-series for all stations (Figure 2e and Figure S3 in Supporting Information S1). However, the advantage of the PCA is to provide the spatial information on the displacement amplitudes (Figure S2a in Supporting Information S1).

We compare the temporal evolution of PC1 with the SPEI-12 index value, averaged over the Po river basin, and with the Po river level measurements provided by the Regional Agency for Environmental Protection of Veneto region (ARPAV; https://wwwold.arpa.veneto.it/arpavinforma/bollettini/dati-storici, Last Access: 24-07-2023). The SPEI-12 quantifies the drought level of the previous 12 months, considering the precipitation and potential evapotranspiration anomalies over 12 months (Figure 1a), which is the most suitable time scale for interannual drought monitoring over a decade (Enyu et al., 2023).

The Po river level time series is filtered adopting the same approach used for the GNSS time-series, retaining only the piecewise trend component (Figure S4 in Supporting Information S1) and not the seasonal ones. On the other hand, SPEI-12 time series does not contain annual variations, since the index is computed as an anomaly over 12 months, then the time series has not been filtered. Figure 3a shows that the geodetic (sign inverted), climatic and hydrological time series are highly temporally correlated, so that geodetic uplift is observed coeval with the drop of the Po river level and the SPEI-12 index, while the geodetic subsidence is observed coeval with the increase of the Po river level and SPEI-12 index, respectively. In particular, the geodetic time series is characterized, besides the minimum in August 2022, by minima also in winter 2012 and 2017, which corresponds to periods of maximum ground uplift and to known major drought episodes (Baronetti et al., 2020). While for the 2012 and 2022 minima there is a good correspondence between GNSS, Po river level and SPEI-12, for the 2017 there is some discrepancy, which is discussed later in Section 4. Focusing on the time interval covering the last drought, we observe that the three de-seasoned time series start decreasing from the beginning of 2021 to mid-2022, after which they invert their sign. As a result, we set the time limits of the drought as 2021.00 and 2022.58 (1 January 2021–1 August 2022), which is represented as the yellow area in Figure 3a.

The vertical displacements associated with PC1 from 2021.00 to 2022.58 are shown in Figure 3b. Most of the stations show positive values (uplift), in accordance with the hypothesis that in dry periods, when the water load is reduced, the GNSS stations record uplift, while in wet periods the water load increases causing a downward motion of the Earth's surface. We find that this is not true for 22 sites, which show an opposite behavior (black triangles in Figure 3b). Maximum uplift, of the order of 7 mm, is observed in the south-eastern portion of the basin and in the northern portion of the Po basin, which correspond to uplift rates, in the considered 2 years, that are much faster than the long-term ones (e.g., Pintori et al., 2022).

3.2. Inversion of Vertical Ground Displacements

The displacements associated with PC1 in the 2021.00–2022.58 time span are inverted using the approach described in Jiang, Hsu, Yuan, Feng, et al. (2022), which estimates water storage variations assuming an elastic response of the Earth to the hydrological load. In order to avoid misinterpretation of the spatial variations of the water storage changes, we exclude from the inversion the 22 stations showing negative vertical displacements (i.e., subsidence, Figure S5 in Supporting Information S1) in the investigated time interval that, following Carlson et al. (2022), are possibly affected by poroelastic processes, causing vertical displacements in the opposite direction compared to the elastic ones. We also exclude from the inversion the GNSS stations that have no observations

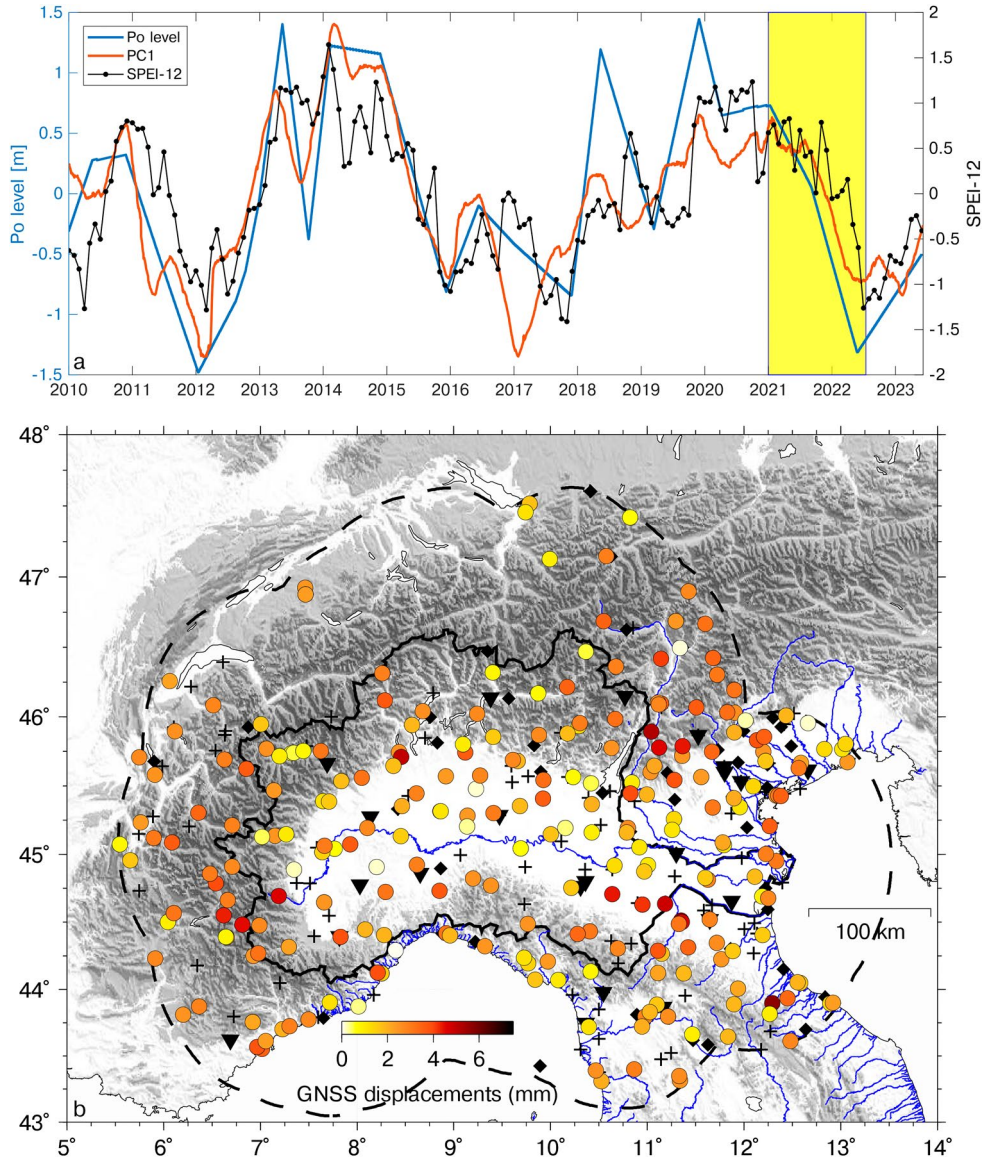

Figure 3. (a) Comparison between the PC1 temporal evolution, the SPEI-12 index and the Po river level. Since PC1 is obtained from detrended Global Navigation Satellite System time series, Po river level and SPEI-12 have also been detrended for consistency. (b) Vertical displacements associated with PC1 during the 2021.00 (January 2021)–2022.58 (August 2022) time interval (yellow panel). The dashed line represents the boundary of the Po river basin, extended by 1°. Black triangles indicate the 22 stations excluded because they show negative displacements; black crosses represent sites with more than 75% of missing data and black diamonds the stations with no records after 2021.0.

recorded in the 2021.00–2022.58 time-span (i.e., do not register displacements potentially associated with the last drought episode investigated in this work). The total number of stations used for the inversion is then 257.

The relationship between the vertical displacements measured by GNSS x and the water mass load u, expressed as EWH, is

$$x = Gu$$

where G is the Green's function matrix using load Love numbers of the preliminary reference earth model (PREM) (Dziewonski & Anderson, 1981) as commonly used in many recent works (e.g., Carlson et al., 2022; Jiang et al., 2021). The final solution for the daily estimates of EWH changes u is

$$u = \left(G^T G + \alpha^2 L^T L\right)^{-1} G^T x$$

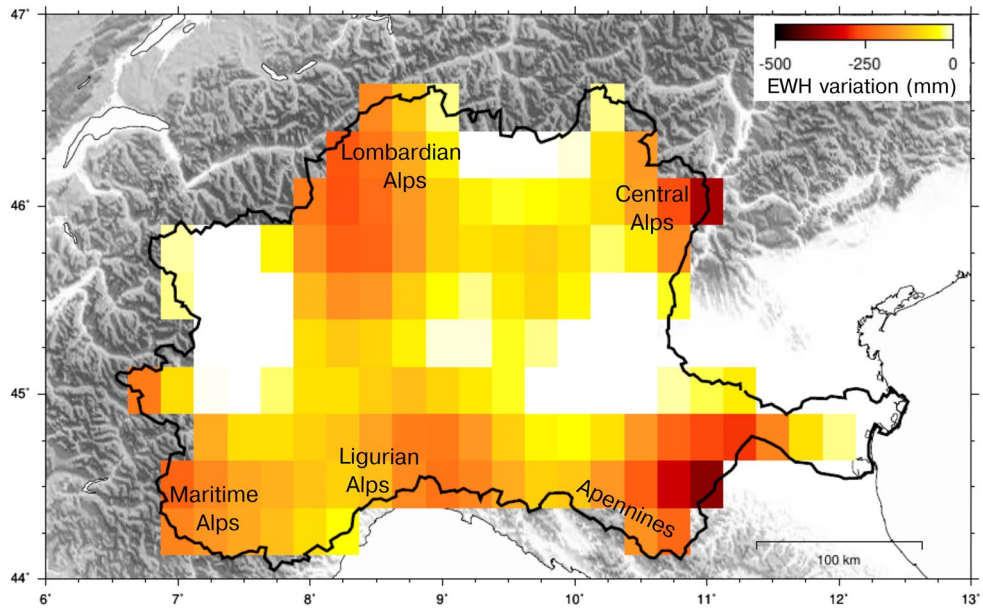

Figure 4. Water loss occurred in the 2021.00–2022.58 time interval in terms of equivalent water height from the inversion of the vertical Global Navigation Satellite System signal.

where $\boldsymbol{L}$ is the Laplacian smoothing matrix and $\boldsymbol{\alpha}$ is the smoothing factor controlling the relative weight between model roughness and data misfit.

We invert the displacements associated with PC1 to estimate EWH on a $0.25° \times 0.25°$ grid. We choose $\alpha = 0.0030$, which is the minimum in the line showing the relation between the sum of squared residuals from cross-validation (CVSS) and the smoothing factor (Figure S6 in Supporting Information S1), and use four neighbor points for calculating the Laplacian matrix during the least-squares inversion.

Figure 4 shows the inverted spatial distribution of water loss, expressed as EWH in mm for the specific time interval shown in yellow in Figure 3. It is worth considering that the temporal evolution of EHW resembles that of PC1 in Figure 3, as the approach adopted assumes that the deformation source (in this case the decrease or increase of hydrological loading) remains static in space, which is a possible limitation of the multivariate statistical approach (see also Gualandi et al., 2016; Kositsky & Avouac, 2010).

A checkerboard test using synthetic inputs is performed to show the ability of the inversion method and the distribution of the GNSS stations to resolve spatial features of water mass variation in a checkerboard pattern, where each mass has dimensions of $1° \times 1°$ and an EWH change of 300 mm (Figure 5a). The inversion performance is evaluated estimating the agreement dR between each grid point of the checkerboard synthetic model within the Po river basin and the results of the inversion (Figure 5a) using the following equation, which estimates the percentage of accuracy:

$$\mathrm{dR} = 1 - \frac{|\mathrm{input} - \mathrm{output}|}{\max(\mathrm{input})}$$

where input is the value of the checkerboard synthetic model, output the value resulting from the inversion and max(input) the maximum value of input, that is, 300 mm. The mean value of dR computed over all the grid points is 0.70, then we can conclude that the accuracy of our inversion, at the resolution of $1° \times 1°$, is 70%. By using smaller patches we find a rapid degradation of the spatial accuracy (Figures 5a and 5b).

It is also worth noting that the spatial distribution of the GNSS station is not uniform, so that the spatial features are not resolved with the same quality over the study area. For example, no data are available in the Switzerland territory, so that the EWH spatial resolution in the north-western portion of the study area is much poorer than the center of the Po basin, where there is a high GNSS station density.

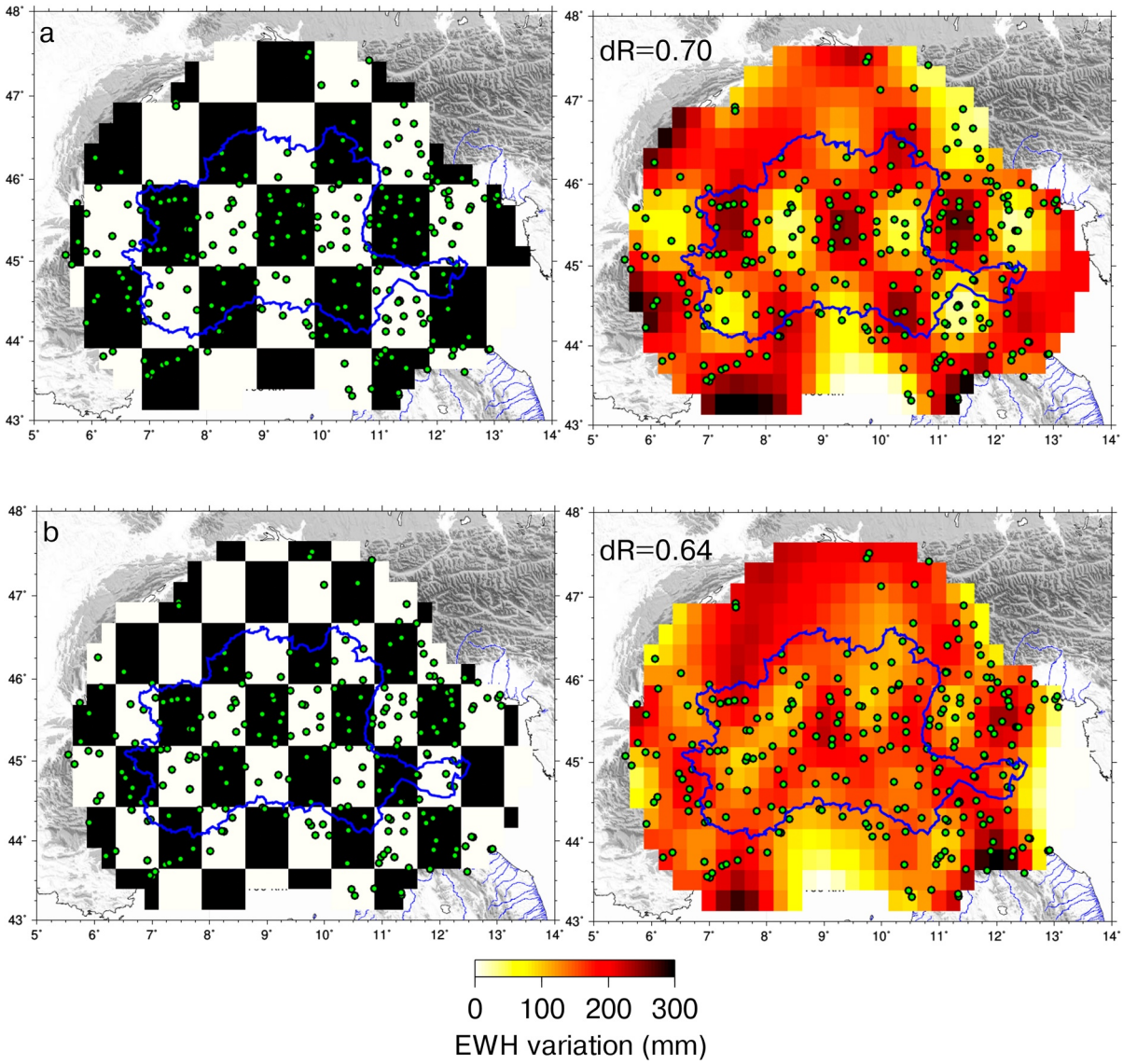

Figure 5. Checkerboard test using synthetic data. (a) Comparison between the checkerboard synthetic model (left) and the results using the inversion method (right) considering a 1.00° spatial resolution. (b) Same as (a) but considering a 0.75° spatial resolution.

4. Discussion

We compare the EWH obtained by inverting the GNSS displacements (EWH_{gnss}) with surface water content (SWC) from GLDAS and with Liquid Water Equivalent Thickness (LWE) from GRACE.

The GLDAS products provide the soil moisture content in the first 2 m of the subsurface, the snow depth water equivalent, the plant canopy surface water and the root zone soil moisture (Rodell et al., 2004). We consider as SWC the sum of these four components, which are provided as 0.25° × 0.25° gridded data set and 3-hr temporal resolution, which are transformed into daily time series by averaging the 3-hourly time series to make them consistent with the daily resolution of EWH_{gnss}.

LWE is computed using the NASA Jet Propulsion Laboratory (JPL) GRACE and GRACE-FO RL06 Mascon solutions (Watkins et al., 2015), but we also show the results obtained using other GRACE products in Supporting Information S1. While the data are here analyzed in a 0.25° × 0.25° grid for consistency with SWC and EWH_{gnss}, the current resolution is 300 km. The temporal resolution of LWE data is monthly and data are missing in correspondence with the gap between the GRACE and GRACE-FO missions, which results in a 11 months gap, from July 2017 to May 2018.

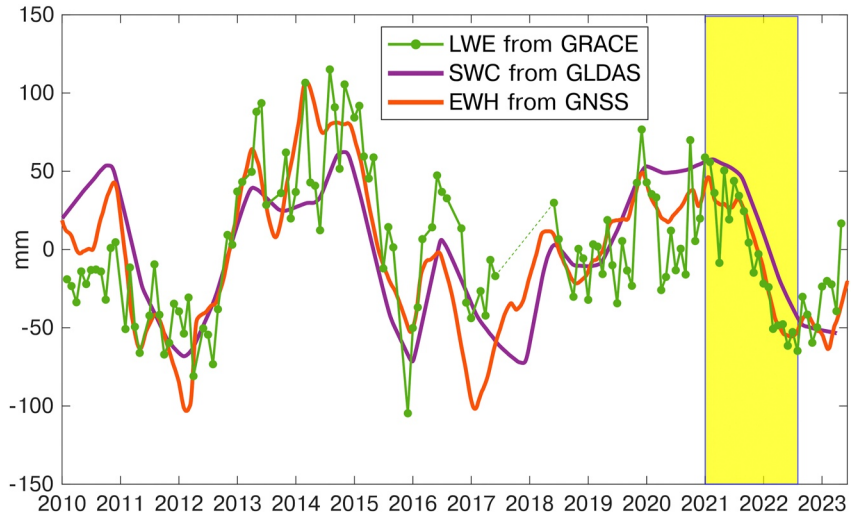

Figure 6. Comparison among the temporal evolutions of the regional-averaged water content expressed as EWH_{gnss} (red), SWC (purple) and Liquid Water Equivalent Thickness (green). Since equivalent water height is obtained from Global Navigation Satellite System detrended data; both Global Land Data Assimilation System and Gravity Recovery and Climate Experiment data have also been detrended for consistency.

The GLDAS products allow an estimate of the water content with a better nominal spatial resolution of EWH_{gnss}, even though the disadvantage is that GLDAS does not take into account groundwater. Importantly, while the GLDAS nominal spatial resolution is 0.25°, its effective resolution may be different due to the assimilation process and the interpolation techniques used to generate gridded data sets. Furthermore, the nominal spatial resolution of GLDAS may not represent the true spatial variability of soil moisture in a context such as the Po river basin, characterized by high topographic gradients. The correct determination of the soil types in regions characterized by heterogeneous landscapes, elevation and land cover, in fact, is complex and this can lead to errors in soil moisture modeling (Bi et al., 2016).

LWE takes into account all TWS components, but with a spatial and temporal resolution much poorer than EWH_{gnss}. We point out that while EWH_{gnss} is inverted on a $0.25° \times 0.25°$ grid, the results of the checkerboard test show that the actual spatial resolution is ∼1°, corresponding to about 100 km (Text S1 in Supporting Information S1). This is consistent with the resolution achieved by Zhang et al. (2016) in the Yunnan region of China and by Fu et al. (2015) in Washington and Oregon. The high spatial density of the southern California GNSS network allowed Carlson et al. (2022) to reach a spatial resolution of 80 km, while when considering larger study areas as in Borsa et al. (2014) and in Ferreira et al. (2019) the spatial resolution decreases to 200–300 km.

We remove the annual and semiannual components in SWC time series using the same approach used for GNSS displacement and Po river level measurements (see Figure S7 in Supporting Information S1), and apply a PCA using one PC on the trend components. Because of the monthly temporal resolution of the GRACE products, LWE data are analyzed using a slightly different strategy: we remove the annual and semiannual components from the original time series instead of estimating the trend components, as done for GNSS and GLDAS time-series.

As for the GLDAS and GNSS data sets, the filtered time series are analyzed with a PCA with one PC. Figure 6 shows the temporal evolutions of the basin-averaged water content expressed as EWH_{gnss}, SWC from GLDAS and LWE from GRACE, while Figure 7 shows the spatial distributions of water loss from January 2010 to August 2022 (2021.00–2022.58, yellow box in Figure 6), estimated from GLDAS and GRACE, respectively. Figure 6 shows that the drought time interval, defined in Section 3.1 and shown in Figure 3a considering the SPEI-12, Po level and GNSS data, is also consistent in SWC and LWE time series from GLDAS and GRACE, respectively. It is worth noting that both SWC and LWE show local minima in 2012 and 2017, with the SWC just a little bit delayed in 2017 compared to the other two products. Considering also the SPEI-12 and the Po river level temporal evolutions shown in Figure 3a, we observe that all the data set considered shows local minima in 2012, 2017 and 2022. The only exception is the SPEI-12, which has a local maximum at the beginning of 2017 and a minimum at the end of 2017. The disagreement between the SPEI-12 temporal evolution and the other products is significant only in this specific time interval, while the overall agreement is good.

10.1029/2023EA003326

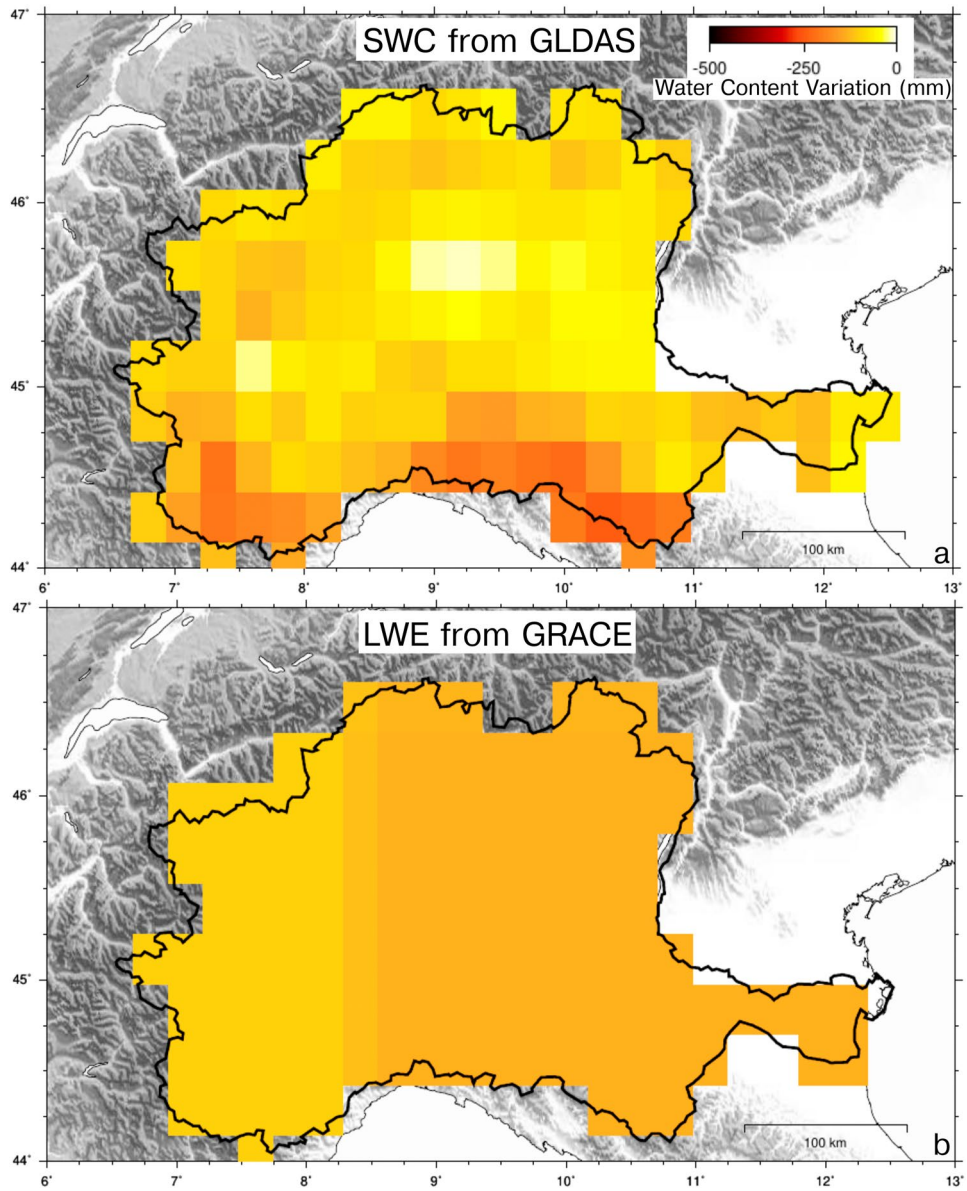

Figure 7. Water loss occurred in the 2021.00–2022.58 time interval in terms of (a) SWC from Global Land Data Assimilation System and (b) Liquid Water Equivalent Thickness from Gravity Recovery and Climate Experiment.

The temporal evolution of the basin-averaged water content estimated by the three models is very similar (Figure 6), suggesting that the water storage variations may be dominated by its superficial content, captured by GLDAS. The spatial distribution of the water loss occurring in the 2021.00–2022.58 time interval (Figure 7) is different depending on the considered data set; nonetheless, averaging on the Po basin surface, we obtain water loss values of the order of about 69, 73, and 90 Gtons from GNSS, GLDAS, and GRACE, respectively in this period.

Figure S8 in Supporting Information S1 shows a comparison in terms of regional-averaged water loss and spatial distribution of LWE thickness change in the 2021.00–2022.58 time interval obtained using the Gravity Information Service of the German Research Center for Geosciences (GRAVIS, Boergens et al., 2020) and the Center for Space Research of the University of Texas (CSR, Save, 2020; Save et al., 2016) GRACE products. Regional averaged water loss values according to CSR and GRAVIS products are 139 and 124 Gtons, respectively. However, because of a higher temporal variability of LWE values from different GRACE products, and in

particular of the CSR one, the water loss estimation may vary significantly with small changes in the considered time interval.

The poor spatial resolution of GRACE measurements makes LWE spatial distribution more uniform than estimates from GLDAS and GNSS and unable to detect possible concentrations of water loss at the scale of the Po river basin. Both SWC and EWH_{gnss} show the largest values in the southern portion of the basin, in the northern Apennines and Maritime and Ligurian Alps.

Differently from SWC, EWH_{gnss} negative anomalies are also large in the northern sector of the Po basin. In particular, in the Lombardian Alps and Prealps, in agreement with the SPEI-12 map (Figure 1), and in the Central Alps, where there might be a side effect with the Adige river basin, where geodetic uplift is among the highest of the study area (Figure 3). The reason for the spatial discrepancies between SWC and EWH_{gnss} estimates can be a consequence of the GLDAS limitations in resolving the spatial distribution of the water loss in the mountain sectors, in the presence of high topographic gradients and diverse use of the soil, as in the investigated area. It is also worth considering that GNSS vertical displacements can contain signals that might cause an incorrect estimation of the water content. In fact, the inversion is made on the displacements reconstructed by the PC1. This statistical approach allows us to identify a common displacement signal that is assumed to have the same temporal evolution in all the GNSS stations, but different amplitudes. The amplitude associated with this signal might be imprecise, especially in GNSS sites characterized by noisy time-series or for stations affected by more localized processes such as water pumping and other anthropogenic activities.

Importantly, estimates of water loss values depend on the Green's function used to invert the displacements data. Several authors (e.g., Argus et al., 2017; Chanard et al., 2014), point out that a gravitating, spherical Earth model is preferred in this context, since non gravitating, half-space models, can understate elastic vertical displacements up to a factor of 2.5. Moreover, the results are not very sensitive to the Earth's structure: assuming two different models for the Earth, PREM and the Gutenberg Bullen A Earth structure (Farrell, 1972), Argus et al. (2017) find that the difference between the displacements caused by a 450 km × 60 km load is only 4%.

5. Conclusions

We analyze vertical ground displacements from GNSS stations located in the Po river basin, a significant and important industrial and agricultural district at European level. We find that inter-annual and multi-annual changes in vertical trends clearly respond to meteo-climatic forcing and serve as a reliable, near real-time, independent approximation of drought indexes. Differently from meteorological drought indicators, the measure of vertical displacements allows estimating the severity of hydrological drought in terms of spatial and temporal evolution of water volume loss, which is crucial for managing the problem of water scarcity. During the last dry period that has affected the study region, from the beginning of 2021 to the summer of 2022, we observe a regional geodetic uplift signal. This uplift reaches values of up to 7 mm and exhibits spatial variations across the area. We interpret this phenomenon as a result of variable water loss and subsequent reduced load, enabling us to estimate the spatial distribution of EWH. We estimate that approximately 70 Gtons of water was lost in the Po river basin from 2021 to August 2022. This estimate aligns with values obtained from GLDAS but is lower than the estimate derived from GRACE. Additionally, while the temporal evolution of EWH estimated by GNSS, GLDAS, and GRACE shows similarities, the spatial patterns differ significantly. EWH_{gnss}, despite a formal resolution of 100 × 100 km, due to a decrease in GNSS stations availability from 2021, still offers the best estimates of water loss in the Po basin.

Our findings are also relevant for studying active tectonics and geodynamics. The Apennines and Alps, in fact, exhibit long-term uplift signals resulting from various multiscale processes (Sternai et al., 2019). Accounting for the hydrological origins of trend variations is crucial to improve accuracy and prevent misinterpretation of transient signals or biases in velocity estimates, especially in case of short time-series.

Future works aim at integrating GNSS with InSAR observations in order to improve the spatial resolution of EWH to a few tens of meters, as demonstrated by Ghorbani et al. (2022), and to collect and analyze in situ measurements, such as water well, when available. This integration would enhance our understanding of the phenomenon and provide more detailed information on water loss and recharge dynamics.

Data Availability Statement

The EWH is estimated by inverting the GNSS data using the GNSS2TWS software (https://github.com/jzshhh/gnss2tws). The code gnss2ewh_main.m was slightly changed and is available at https://doi.org/10.6084/m9.figshare.24551167.v1. The trend filtering on the time series is performed using the L1tool software (https://github.com/wudingcheng/l1tool). The stacking of the GNSS time series is performed using the GNSS_TS_NRS code (https://github.com/CL-Xiong/GNSS-TS-NRS, He et al., 2020). GLDAS data was downloaded from https://disc.gsfc.nasa.gov/datasets/GLDAS_NOAH025_3H_2.1/summary?keywords=GLDAS (Beaudoing and Rodell, 2020) and available at https://doi.org/10.6084/m9.figshare.24551167.v1 for this study region (GLDAS_NOAH025_until202303daily.nc4). GRACE data provided by the Center for Space Research of the University of Texas (CSR) was downloaded from http://www2.csr.utexas.edu/grace (https://doi.org/10.15781/cgq9-nh24) and available at https://doi.org/10.6084/m9.figshare.24551167.v1 for this study region (CSR_GRACE_6,13,43,47.nc). GRACE/GRACE-FO Mascon data provided by the NASA Jet Propulsion Laboratory (JPL) are available at http://grace.jpl.nasa.gov and at https://doi.org/10.6084/m9.figshare.24551167.v1 for this study region (GRCTellus.JPL.200204_202305.GLO.RL06.1M.MSCNv03_PoBasin_0.25.nc). GRACE data provided by the Gravity Information Service of the German Research Center for Geosciences (GRAVIS) are available at https://doi.org/10.5880/COST-G.GRAVIS_01_L3_TWS and at https://doi.org/10.6084/m9.figshare.24551167.v1 for this study region (GRAVIS-3_PoBasin_0.25.nc). The data set of the displacements caused by the atmospheric loading are downloaded from http://rz-vm115.gfz-potsdam.de:8080/repository/ (LSDM-based model). SPEI-12 data was downloaded from https://spei.csic.es/map/maps.html#months=1#month=0#year=2023GNSS. The data set used to generate Figure 1a is spei12_full, while Figure 3a is generated using spei12_PoBasin025.nc. Both are available at https://doi.org/10.6084/m9.figshare.24551167.v1. GNSS time series data are available from https://doi.org/10.6084/m9.figshare.24486841.v1. The maps have been made using the GMT software (Wessel et al., 2019). The Po river level measurements are provided by the Regional Agency for Environmental Protection of Veneto region (ARPAV; https://wwwold.arpa.veneto.it/arpavinforma/bollettini/dati-storici) and available at https://doi.org/10.6084/m9.figshare.24551167.v1 (Po_level_updated23_L1tool_output_2023.txt). The Principal Component Analysis on GRACE and GLDAS data is performed using the vbICA code (https://data.mendeley.com/datasets/n92vwbg8zt/1) (Gualandi & Pintori, 2020). The MIDAS software is available at http://geodesy.unr.edu/MIDAS_release/. The repository https://doi.org/10.6084/m9.figshare.24551167.v1 also contains:

- the code (filter_NTAL.m) and data (ESMGFZ_NTAL_cf_v1.0_2010_202307_daily_full.nc) to remove the effect of the atmospheric loading from the time series;
- the polygons of the Po river basin (Po_River_Basin_Italy.gpx) and of the Po river basin extended by 1° (PO_basin_buffer_1.0.dat);
- the code display_results.m, which allows us to generate the figures (or input data for the figures) 1c, 2e, 3b, 4, 6, 7, and S8. This code should be placed in the same directory of gnss2ewh_main.m. Please note that the code reads four .mat files containing the results of the PCA decomposition on GRACE and GLDAS data. These files are also available in this repository;
- the function checkerboard_test.m, which is a modification of the function checkerboard_test.m available in https://github.com/jzshhh/gnss2tws. This new function allows to generate the inputs for plotting Figure 5.

Acknowledgments
This work was supported by the INGV Departmental Strategic Project MUSE. We thank GNSS data providers (see Serpelloni et al. (2022) for references), and in particular private networks providers. Some of the figures are created using the Generic Mapping Tools (GMT) software (Wessel et al., 2019).

References

Argus, D. F., Fu, Y., & Landerer, F. W. (2014). Seasonal variation in total water storage in California inferred from GPS observations of vertical land motion. *Geophysical Research Letters*, *41*(6), 1971–1980. https://doi.org/10.1002/2014GL059570

Argus, D. F., Landerer, F. W., Wiese, D. N., Martens, H. R., Fu, Y., Famiglietti, J. S., et al. (2017). Sustained water loss in California's mountain ranges during severe drought from 2012 to 2015 inferred from GPS. *Journal of Geophysical Research: Solid Earth*, *122*(12), 10559–10585. https://doi.org/10.1002/2017JB014424

Baronetti, A., González-Hidalgo, J. C., Vicente-Serrano, S. M., Acquaotta, F., & Fratianni, S. (2020). A weekly spatio-temporal distribution of drought events over the Po Plain (North Italy) in the last five decades. *International Journal of Climatology*, *40*(10), 4463–4476. https://doi.org/10.1002/joc.6467

Beaudoing, H., Rodell, M., & NASA/GSFC/HSL. (2020). *GLDAS Noah land surface model L4 3 hourly 0.25 x 0.25 degree V2.1, Greenbelt, Maryland, USA*. Goddard Earth Sciences Data and Information Services Center (GES DISC). https://doi.org/10.5067/E7TYRXPJKWOQ

Bi, H., Ma, J., Zheng, W., & Zeng, J. (2016). Comparison of soil moisture in GLDAS model simulations and in situ observations over the Tibetan Plateau. *Journal of Geophysical Research: Atmospheres*, *121*(6), 2658–2678. https://doi.org/10.1002/2015jd024131

Blewitt, G., Kreemer, C., Hammond, W. C., & Gazeaux, J. (2016). MIDAS robust trend estimator for accurate GPS station velocities without step detection. *Journal of Geophysical Research: Solid Earth*, *121*(3), 2054–2068. https://doi.org/10.1002/2015JB012552

Boergens, E., Dobslaw, H., & Dill, R. (2020). *COST-G GravIS RL01 continental water storage anomalies. V. 0005*. GFZ Data Services. https://doi.org/10.5880/COST-G.GRAVIS_01_L3_TWS

Borsa, A. A., Agnew, D. C., & Cayan, D. R. (2014). Remote Hydrology. Ongoing drought-induced uplift in the Western United States. *Science*, *345*(6204), 1587–1590. https://doi.org/10.1126/science.1260279

Boyko, O., Reggiani, P., & Todini, E. (2022). Post-processing climate projections of precipitation for the Po river basin: Will Italy's North become water-constrained? *Hydrology Research*, *53*(11), 1414–1427. https://doi.org/10.2166/nh.2022.063

Carlson, G., Werth, S., & Shirzaei, M. (2022). Joint inversion of GNSS and GRACE for terrestrial water storage change in California. *Journal of Geophysical Research: Solid Earth*, *127*(3), e2021JB023135. https://doi.org/10.1029/2021JB023135

Chanard, K., Avouac, J. P., Ramillien, G., & Genrich, J. (2014). Modeling deformation induced by seasonal variations of continental water in the Himalaya region: Sensitivity to Earth elastic structure. *Journal of Geophysical Research: Solid Earth*, *119*(6), 5097–5113. https://doi.org/10.1002/2013JB010451

Dill, R., & Dobslaw, H. (2013). Numerical simulations of global-scale high-resolution hydrological crustal deformations. *Journal of Geophysical Research: Solid Earth*, *118*(9), 5008–5017. https://doi.org/10.1002/jgrb.50353

Dziewonski, A. M., & Anderson, D. L. (1981). Preliminary reference Earth model. *Physics of the Earth and Planetary Interiors*, *25*(4), 297–356. https://doi.org/10.1016/0031-9201(81)90046-7

Enyu, D., Chen, F., Jia, H., Wang, L., & Yang, A. (2023). Spatiotemporal evolution and hysteresis analysis of drought based on rainfed-irrigated Arable Land. *Remote Sensing*, *15*(6), 1689. https://doi.org/10.3390/rs15061689

Farrell, W. E. (1972). Deformation of the Earth by surface loads. *Reviews of Geophysics and Space Physics*, *10*(3), 761–797. https://doi.org/10.1029/rg010i003p00761

Ferreira, V., Ndehedehe, C., Montecino, H., Yong, B., Yuan, P., Abdalla, A., & Mohammed, A. (2019). Prospects for imaging terrestrial water storage in South America using daily GPS observations. *Remote Sensing*, *11*(6), 679. https://doi.org/10.3390/rs11060679

Fu, Y., Argus, D. F., & Landerer, F. W. (2015). GPS as an independent measurement to estimate terrestrial water storage variations in Washington and Oregon. *Journal of Geophysical Research: Solid Earth*, *120*(1), 552–566. https://doi.org/10.1002/2014JB011415

Ghorbani, Z., Khosravi, A., Maghsoudi, Y., Mojtahedi, F. F., Javadnia, E., & Nazari, A. (2022). Use of InSAR data for measuring land subsidence induced by groundwater withdrawal and climate change in Ardabil Plain, Iran. *Scientific Reports*, *12*(1), 13998. https://doi.org/10.1038/s41598-022-17438-y

Gualandi, A., & Pintori, F. (2020). *vbICA code*. Mendeley Data, V1. https://doi.org/10.17632/n92vwbg8zt.1

Gualandi, A., Serpelloni, E., & Belardinelli, M. E. (2014). Space-time evolution of crustal deformation related to the Mw 6.3, 2009 L'Aquila earthquake (central Italy) from principal component analysis inversion of GPS position time-series. *Geophysical Journal International*, *197*(1), 174–191. https://doi.org/10.1093/gji/ggt522

Gualandi, A., Serpelloni, E., & Belardinelli, M. E. (2016). Blind source separation problem in GPS time series. *Journal of Geodesy*, *90*(4), 323–341. https://doi.org/10.1007/s00190-015-0875-4

He, X., Yu, K., Montillet, J.-P., Xiong, C., Lu, T., Zhou, S., et al. (2020). GNSS-TS-NRS: An open-source MATLAB-based GNSS time series noise reduction software. *Remote Sensing*, *12*(21), 3532. https://doi.org/10.3390/rs12213532

Jiang, Z., Hsu, Y.-J., Yuan, L., Feng, W., Yang, X., & Tang, M. (2022). GNSS2TWS: An open-source MATLAB-based tool for inferring daily terrestrial water storage changes using GNSS vertical data. *GPS Solutions*, *26*(4), 114. https://doi.org/10.1007/s10291-022-01301-8

Jiang, Z., Hsu, Y.-J., Yuan, L., & Huang, D. (2021). Monitoring time-varying terrestrial water storage changes using daily GNSS measurements in Yunnan, southwest China. *Remote Sensing of Environment*, *254*, 112249. https://doi.org/10.1016/j.rse.2020.112249

Jiang, Z., Hsu, Y. J., Yuan, L., Tang, M., Yang, X., & Yang, X. (2022). Hydrological drought characterization based on GNSS imaging of vertical crustal deformation across the contiguous United States. *The Science of the Total Environment*, *823*, 153663. https://doi.org/10.1016/j.scitotenv.2022.153663

Knappe, E., Bendick, R., Martens, H. R., Argus, D. F., & Gardner, W. P. (2019). Downscaling vertical GPS observations to derive watershed-scale hydrologic loading in the northern Rockies. *Water Resources Research*, *55*(1), 391–401. https://doi.org/10.1029/2018WR023289

Kositsky, A. P., & Avouac, J. P. (2010). Inverting geodetic time series with a principal component analysis-based inversion method. *Journal of Geophysical Research*, *115*(B3), B03401. https://doi.org/10.1029/2009JB006535

Montanari, A., Nguyen, H., Rubinetti, S., Ceola, S., Galelli, S., Rubino, A., & Zanchettin, D. (2023). Why the 2022 Po River drought is the worst in the past two centuries. *Science Advances*, *9*(32), eadg8304. https://doi.org/10.1126/sciadv.adg8304

Pintori, F., Serpelloni, E., & Gualandi, A. (2022). Common-mode signals and vertical velocities in the greater Alpine area from GNSS data. *Solid Earth*, *13*(10), 1541–1567. https://doi.org/10.5194/se-13-1541-2022

Rodell, M., Houser, P. R., Jambor, U., Gottschalck, J., Mitchell, K., Meng, C. J., et al. (2004). The global land data assimilation system. *Bulletin of the American Meteorological Society*, *85*(3), 381–394. https://doi.org/10.1175/BAMS-85-3-381

Save, H. (2020). CSR GRACE and GRACE-FO RL06 Mascon solutions v02. https://doi.org/10.15781/cgq9-nh24

Save, H., Bettadpur, S., & Tapley, B. D. (2016). High-resolution CSR GRACE RL06 mascons version 2. *Journal of Geophysical Research: Solid Earth*, *121*(10), 7547–7569. https://doi.org/10.1002/2016JB013007

Serpelloni, E., Cavaliere, A., Martelli, L., Pintori, F., Anderlini, L., Borghi, A., et al. (2022). Surface velocities and strain-rates in the Euro-Mediterranean region from massive GPS data processing. *Frontiers in Earth Science*, *10*. https://doi.org/10.3389/feart.2022.907897

Sternai, P., Sue, C., Husson, L., Serpelloni, E., Becker, T. W., Willett, S. D., et al. (2019). Present-day uplift of the European Alps: Evaluating mechanisms and models of their relative contributions. *Earth-Science Reviews*, *190*, 589–604. https://doi.org/10.1016/j.earscirev.2019.01.005

Vicente-Serrano, S. M., Beguería, S., & López-Moreno, J. I. (2010). A multiscalar drought index sensitive to global warming: The standardized precipitation evapotranspiration index. *Journal of Climate*, *23*(7), 1696–1718. https://doi.org/10.1175/2009JCLI2909.1

Watkins, M. M., Wiese, D. N., Yuan, D.-N., Boening, C., & Landerer, F. W. (2015). Improved methods for observing Earth's time variable mass distribution with GRACE using spherical cap mascons. *Journal of Geophysical Research: Solid Earth*, *120*(4), 2648–2671. https://doi.org/10.1002/2014JB011547

Wessel, P., Luis, J. F., Uieda, L., Scharoo, R., Wobbe, F., Smith, W. H. F., & Tian, D. (2019). The generic mapping tools version 6. *Geochemistry, Geophysics, Geosystems*, *20*(11), 5556–5564. https://doi.org/10.1029/2019GC008515

White, A. M., Gardner, W. P., Borsa, A. A., Argus, D. F., & Martens, H. R. (2022). A review of GNSS/GPS in hydrogeodesy: Hydrologic loading applications and their implications for water resource research. *Water Resources Research*, *58*(7), e2022WR032078. https://doi.org/10.1029/2022WR032078

Wu, D., Yan, H., & Yuan, S. (2018). L1 regularization for detecting offsets and trend change points in GNSS time series. *GPS Solutions*, *22*(3), 88. https://doi.org/10.1007/s10291-018-0756-4

Zhang, B., Yao, Y., Fok, H. S., Hu, Y., & Chen, Q. (2016). Potential seasonal terrestrial water storage monitoring from GPS vertical displacements: A case study in the lower three-rivers headwater region, China. *Sensors*, *16*(9), 1526. https://doi.org/10.3390/s16091526

Zhu, H., Chen, K., Hu, S., Liu, J., Shi, H., Wei, G., et al. (2023). Using the global navigation satellite system and precipitation data to establish the propagation characteristics of meteorological and hydrological drought in Yunnan, China. *Water Resources Research*, *59*(4), e2022WR033126. https://doi.org/10.1029/2022WR033126